coatings

MDPI

Communication

Nickel-Cobalt-Iron Ternary Layered Double Hydroxide Nanoarrays for Superior Performance of Electrocatalytic Water Splitting

Zhi Lu [1,2,3,*], Zhihao Zhou [1,2,3], Shilin Li [1,2,3], Guoqing Huang [1], Tianwen He [1], Jiaqi Cai [1], Mingyang Jin [1], Yiting Li [1], Xuefeng Zhang [4], Shuaifang Li [4], Chong Chen [1] and Guangxin Wang [1,2,3,*]

[1] School of Materials Science and Engineering, Henan University of Science and Technology, Luoyang 471003, China
[2] Henan Engineering Research Center for High Purity Materials and Sputtering Targets, Luoyang 471003, China
[3] Luoyang Key Laboratory of High Purity Materials and Sputtering Targets, Luoyang 471003, China
[4] Fonlink Photoelectric (Luo Yang) Co., Ltd., Luoyang 471000, China
* Correspondence: luzhi02013@163.com (Z.L.); wgx0358@163.com (G.W.)

Abstract: The design of high-performance and low-cost oxygen evolution reaction (OER) electrocatalysts is crucial for environment friendly hydrogen production. Some transition metals have been proven to be good substitutes for noble metals due to their unique electronic structural characteristics and good electrocatalytic performances, with examples including nickel and cobalt, which are usually used to prepare OER electrocatalysts. In this work, we synthesized three-dimensional Ni-Co-Fe ternary layered double hydroxide nanosheet array electrocatalysts via hydrothermal process. Iron element was introduced into the Ni-Co based hydroxide. The ternary layered double hydroxide has a nanoarrays microstructure. Theoretical analysis confirms that by adjusting the ratio of Ni/Co/Fe, the microstructure of the catalyst changes significantly. Attributed to the special nanostructure, the catalysts show superior catalytic activities in oxygen evolution reaction (OER). The results show that a small overpotential of 222 mV at the current density of 20 $mA{\cdot}cm^{-2}$ for the OER in 1.0 M KOH is acquired. A small Tafel slope of 61.22 $mVdec^{-1}$ and a maximum specific capacitance of 239 Fg^{-1} are also obtained.

Keywords: oxygen evolution reaction; nanoarrays; Ni-Co based; electrocatalyst

Citation: Lu, Z.; Zhou, Z.; Li, S.; Huang, G.; He, T.; Cai, J.; Jin, M.; Li, Y.; Zhang, X.; Li, S.; et al. Nickel-Cobalt-Iron Ternary Layered Double Hydroxide Nanoarrays for Superior Performance of Electrocatalytic Water Splitting. *Coatings* **2023**, *13*, 726. https://doi.org/10.3390/coatings13040726

Academic Editor: Emerson Coy

Received: 9 February 2023
Revised: 21 March 2023
Accepted: 26 March 2023
Published: 2 April 2023

1. Introduction

The problems associated with global warming resulting from the excessive consumption of fossil fuels are becoming serious, so the transition toward renewable energy is becoming more and more urgent [1,2]. Among the many new and renewable resources, although solar and wind energy are considered to be the lowest cost, their transportation and storage represent a prominent problem [3]. As a clean energy carrier, hydrogen has been considered an excellent candidate to replace fossil fuels [4,5]. Moreover, it can also be used as a form of energy storage that can be converted from excess supplies of other renewable energy, such as solar, and transported to other area via pipelines or compressed canister [6]. Water electrolysis is considered to be a sustainable hydrogen production technology due to its simple process, as well as the wide availability of raw and renewable materials [7]. However, the efficiency of water electrolysis is determined by the oxygen evolution reaction (OER) in anodic processes due to its inert chemical reaction dynamics [8]. Therefore, it is crucial to design high-performance OER catalysts to promote the reaction efficiency of the anodic processes [9,10]. In general, the most effective catalysts are the noble metals and their oxides, such as Pt, RuO_2, and IrO_2, but the high cost of raw materials severely limits their commercial application [11,12].

To overcome this problem, some transition metals, such as Ni and Co, have attracted enormous attention due to their abundance on Earth and excellent catalytic performance [13–15].

The layered double hydroxides (LDHs) of transition metals have shown especially excellent electrochemical performance in electrocatalytic water splitting [16]. Compared to one-dimensional nanostructures, such as nanowires and nanorods, the two-dimensional nanosheet microstructures of LDH have a large surface area and high exposure of active sites [17]. The large surface area can provide more charge transfer channels for the hydrolysis reaction [18]. The catalytic activity of the LDH-based electrocatalysts can be improved by the regulation of the microstructure, such as ionic doping and the introduction of defects, can increase the active sites for catalysts, and can improve the performance of the electrocatalyst [19–21]. Recently, many types of LDH, such as NiMo-LDH, NiFe-LDH, and NiAl-LDH, have been designed, and good performances have been obtained [22–24]. For instances, Wang et al. designed novel hierarchical coral-like Ni-Mo sulfides on Ti mesh through hydrothermal and sulfuration processes; the unique nanostructure showed excellent electrocatalytic performance in both hydrogen evolution and urea oxidation reactions. In 1.0 M KOH, only a cell voltage of 1.59 V was required to deliver 10 $mA \cdot cm^{-2}$ current density [22]. Liu et al. prepared a single layer structure NiFe-LDH by water plasma [23]. They found that the exfoliation of LDH can expose more active sites and multivacancies, which can enhance the electrocatalytic activity of the catalysis. The electrocatalyst showed an ultralow overpotential of 232 mV at 10 mA cm^{-2} and Tafel slope of 36 $mVdec^{-1}$. Wang et al. synthesized NiAl-LDH that dispersed on the surface of graphene by co-deposition method. The catalyst showed a capacitance of 213.57 Fg^{-1} at 1 Ag^{-1} current density, and kept nearly 100% of the original capacitance after 1000 cycles [24,25].

Many investigations have found that the excellent electrocatalytic performance of transition metal compounds was attributed to their electronic structure [26,27]. The electronic structure of the compound always depends on the e_g orbital of transition metal-based materials, the valence state, the spin state, and the covalent bond, especially between O and the transition metal elements [28,29]. The electron transfer of the electrocatalytic reaction is largely dependent on the band structure at the Fermi level, the electronic orbit of the transition metal ions, the carrier concentration, the density of states, and so on [30,31].

The upshift of the d-band center to the Fermi level means that the binding between the catalyst and the adsorbates becomes stronger [32]. The carrier concentration and the electrical conductivity will become higher when there is a higher density of states near the Fermi level. The electrical conductivity and catalytic characteristics can be improved through narrowing the bandgap, since the charge transfer and reaction kinetics can be boosted by a higher electrical conductivity [33]. Therefore, how to tune the electronic configuration and enhance the intrinsic electroactivity of electrocatalysts becomes a hot research topic. Many strategies have been studied, such as heteroatom doping [33], vacancies [34], heterostructures [35], strain engineering [36], and phase transitions [37].

In this work, we synthesized Fe-doped Ni-Co LDH nanoarrays on Ni foam substrate by a one-step hydrothermal method. The method is easy to implement and contributes to the regulating of the microstructure and properties of the material. The unique nanoarray microstructure can offer more active sites for the electrolytic reaction. Through adjusting the doping amount of the Fe element, the electrocatalytic performance of the catalyst can be controlled. An ultralow overpotential of 184 mV at 10 $mAcm^{-2}$ and a low Tafel slope of 61 mV dec^{-1} were obtained in 1.0 M KOH. Attributable to the use of non-noble metals, the work is low cost and is beneficial to put into industrial application. These findings provide valuable insights into the design of novel Ni-Co-based electrocatalysts, and may supply distinctive strategies for designing low-cost electrocatalysts with high performance for the purpose of OER and other catalytic reactions.

2. Materials and Methods

2.1. Materials

Nickel nitrate hexahydrate [$Ni(NO_3)_2 \cdot 6H_2O$, AR], cobaltous nitrate hexahydrate [$Co(NO_3)_2 \cdot 6H_2O$, AR], and ferric nitrate nonahydrate [$Fe(NO_3)_3 \cdot 9H_2O$, AR] were pro-

vided by Shanghai Aladdin Biochemical Technology Co., Ltd. (Shanghai, China). Ni foam (NF) was provided by Beijing Tianmei Hechuang Technology Co., Ltd. (Beijing, China). Urea ($CO(NH_2)_2$, AR) and potassium hydroxide (KOH, AR) were bought from Sinopharm Chemical Reagent Co., Ltd. (Shanghai, China). The hydrolysis of urea can provide OH^- and CO_3^{2-}, which were necessary for the products of this work. All aqueous solutions were prepared using deionized water.

2.2. Electrocatalyst Synthesis

The Fe-doped Ni-Co LDH nanoarrays were synthesized on Ni foam substrate by hydrothermal method as follows. After ultrasonic cleaning for 10 min with a 3 M HCl, a piece of Ni foam (NF 2 cm × 2 cm) was carefully washed several times using ethanol and deionized water in turn to get rid of the surface oxides. Afterward, NF was dried in a vacuum oven. For a typical synthesis, 4 mmol $Ni(NO_3)_2{\cdot}6H_2O$, 4 mmol $Co(NO_3)_2{\cdot}6H_2O$, 0–3 mmol $Fe(NO_3)_3{\cdot}9H_2O$, and 10 mmol urea were dissolved in 60 mL of deionized water under continuous stirring. After 15 min, the mixed solution and the pretreated NF were transferred into a 200 mL polytetrafluoroethylene reaction kettle with stainless steel sleeve. The reactor was heated at 120 °C for 10 h. The samples were washed several times with ethanol and deionized water after they were cooled down to room temperature and were vacuum-dried at 60 °C overnight. By controlling the concentration of $Fe(NO_3)_3{\cdot}9H_2O$, the ratio of Ni:Co:Fe was adjusted to optimize the performance of the electrocatalyst. According to the ratio of Ni:Co:Fe, the samples can be denoted as NiCo-LDH, Ni_4Co_4Fe-LDH, $Ni_4Co_4Fe_2$-LDH, and $Ni_4Co_4Fe_3$-LDH.

2.3. Material Characterizations

X-ray diffraction (XRD) patterns of the materials were obtained through a Bruker-AXS D8 Advance (BRUKER, Ltd., Kyoto, Japan) ray diffractometer with CuKα radiation and scanning speed of 6°/min in 2θ ranging from 5 to 80 degrees. The morphology and elemental analysis of the materials were examined by field emission scanning electron microscopy (FESEM, JSM-7800F, JEOL Ltd., Tokyo, Japan).

2.4. Electrochemical Characterization of Materials

The electrochemical measurements were performed on a three-electrode setup using a CHI-660D electrochemical analyzer (CHI Instruments, Shanghai, China) at room temperature. A platinum strip and Ag/AgCl were used as the counter and reference electrodes, respectively. The reference electrode was filled by saturated KCl solution. The potentials were converted to reversible hydrogen electrodes (RHEs) according to the following formula: E(RHE) = E(Ag/AgCl) + 0.1989 + 0.0591 × pH. For this research, 1 M KOH (pH = 13.7) was used as an electrolyte. The series of as-prepared electrocatalysts were applied as the working electrodes. The overpotentials of OER were calculated by the following equation: η(V) = ERHE − 1.23. The electrochemical properties of the materials were evaluated by cyclic voltammetry (CV) and electrochemical impedance spectroscopy (EIS) techniques. The scan rate of 2 mVs^{-1} and iR compensation were adopted for linear sweep voltammetry (LSV) curves. Electrochemical impedance spectroscopy (EIS) measurements were tested in the frequency range of 0.01–104 Hz. The scan rate of the cyclic voltammetry (CV) ranged from 2 to 10 mV/s. Specific capacitance (Cp) values were calculated based on the following formula [24]:

$$C = \frac{\int_{V_1}^{V_2} Idv}{2\,m\nu(V_2 - V_1)} \quad (1)$$

where C is the specific capacitance (F/g), I is the current (A), m is the mass of the active material of the electrode (g), V_1 and V_2 are the initial and upper potential of the cyclic voltammetry (CV), respectively, and ν is the scan rate of CV.

3. Results and Discussion

3.1. Structural and Morphological Characterization

The crystal structure of the Ni-Co-Fe layered double hydroxide samples were investigated by X-ray diffraction. As shown in Figure 1, there are three sharp diffraction peaks at 2θ = 44.5°, 51.8°, and 76.4°, which correspond to NF (JCPDF No.04-0850). Moreover, there are still some weaker peaks at lower diffraction angles, such as at 2θ = 11.6°, 23°, 34°, and 39°, which correspond to polymetallic hydroxide, such as $3Ni(OH)_2 \cdot 2H_2O$(JCPDF No.22-0444), reevesite ($Ni_6Fe_2(CO_3)(OH)_{16} \cdot 4H_2O$, JCPDF No.26- 1286), and cobalt nickel carbonate hydroxide hydrate ($Ni_{0.75}Co_{0.25}(CO_3)_{0.125}(OH)_2 \cdot 0.38H_2O$,

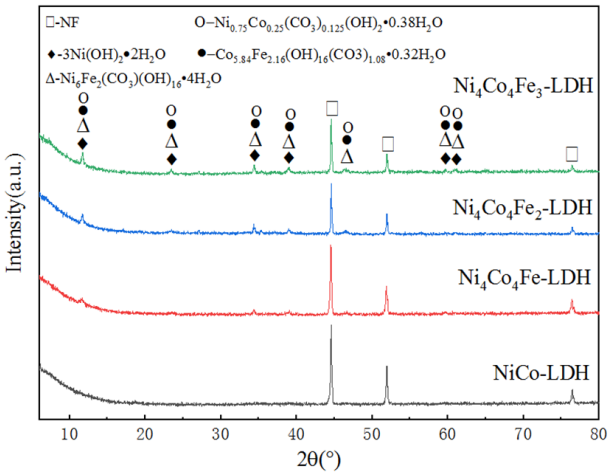

Figure 1. XRD patterns of the as-prepared samples.

It can be seen that the ternary layered double hydroxide was successfully synthesized on the NF substrate. When iron is added, the structure of the material changes significantly. When there is no iron, there is only some hexagonal $3Ni(OH)_2 \cdot 2H_2O$ on the substrate, and the degree of crystallization is lower, as can be seen from the weak peak of $3Ni(OH)_2 \cdot 2H_2O$ in the XRD patterns of NiCo-LDH (Figure 1). With increasing iron, the degree of crystallization is improved significantly, and an abundant of other hexagonal compounds, such as $Ni_6Fe_2(CO_3)(OH)_{16} \cdot 4H_2O$, $Ni_{0.75}Co_{0.25}(CO_3)_{0.125}(OH)_2 \cdot 0.38H_2O$, and $Co_{5.84}Fe_{2.16}(OH)_{16}(CO_3)_{1.08} \cdot 0.32H_2O$, is produced, according to the obvious peaks in the XRD patterns of $Ni_4Co_4Fe_3$-LDH (Figure 1) and the JCPDF cards of these compounds.

The low-magnification morphologies of the samples were observed through FESEM (Figure 2). As shown in Figure 2, the electrocatalysts have a nanostructure. The high-magnification morphologies of the samples are shown in Figure 3. As shown in Figure 3, when doped in a small amount of Fe element, the microstructure of the electrocatalyst transforms from a nanorod to a nanoneedle. However, when there is an excess of Fe element, the microstructure will turn into a nanosheet, as shown in Figure 3d. The parameters of the samples are shown in Table 1. As can be seen, when the iron is increased to a moderate amount, the length-diameter ratio of the nanorods increases from 15 to 23. These features can increase the active sites for electrochemical reactions, and are conducive to the migration of electrons into the catalyst during the OER process. This contributes to improving the performance of electrocatalytic hydrolysis [38].

Table 1. The parameters of the samples.

Samples	Length (μm)	Diameter (nm)	Ratio of L/D
NiCo-LDH/NF	0.9	60	15
Ni_4Co_4Fe-LDH	0.9	50	18
$Ni_4Co_4Fe_2$-LDH	0.7	30	23
$Ni_4Co_4Fe_3$-LDH	-	-	-

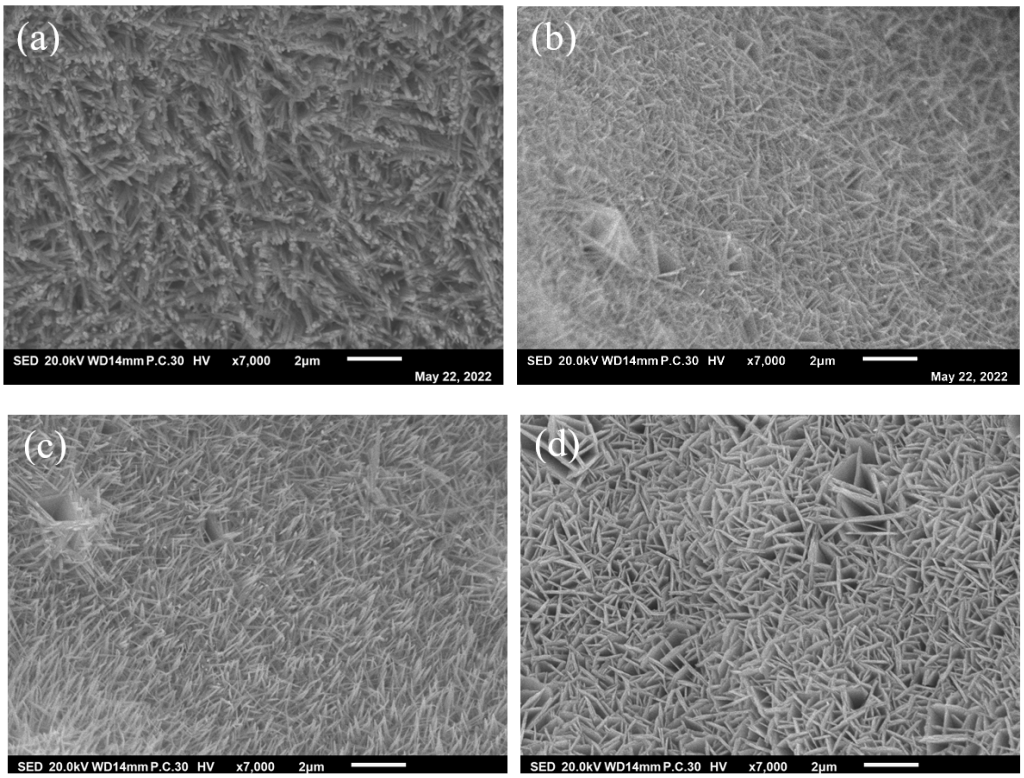

Figure 2. Low magnification of (**a**) NiCo-LDH/NF, (**b**) Ni_4Co_4Fe-LDH/NF, (**c**) $Ni_4Co_4Fe_2$-LDH/NF, and (**d**) $Ni_4Co_4Fe_3$-LDH/NF nanoarrays.

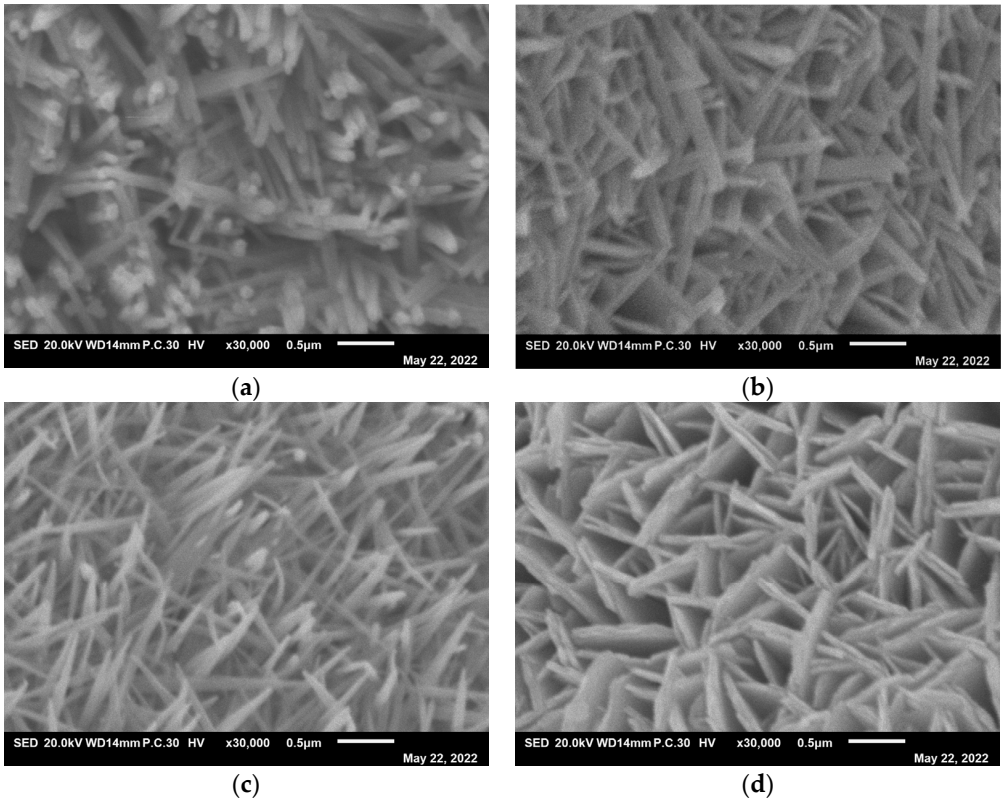

Figure 3. High magnification of (**a**) NiCo-LDH/NF, (**b**) Ni_4Co_4Fe-LDH/NF, (**c**) $Ni_4Co_4Fe_2$-LDH/NF, and (**d**) $Ni_4Co_4Fe_3$-LDH/NF nanostructures.

EDS analysis of $Ni_4Co_4Fe_2$-LDH/NF nanoarrays was carried out through FESEM (Figure 4). As shown in Figure 4, the elements of Ni, Co, Fe, and O distribute uniformly on the surface of the nanostructure, confirming that the surface composition of the $Ni_4Co_4Fe_2$-LDH/NF is relatively uniform, which ensures the stability of catalytic performance.

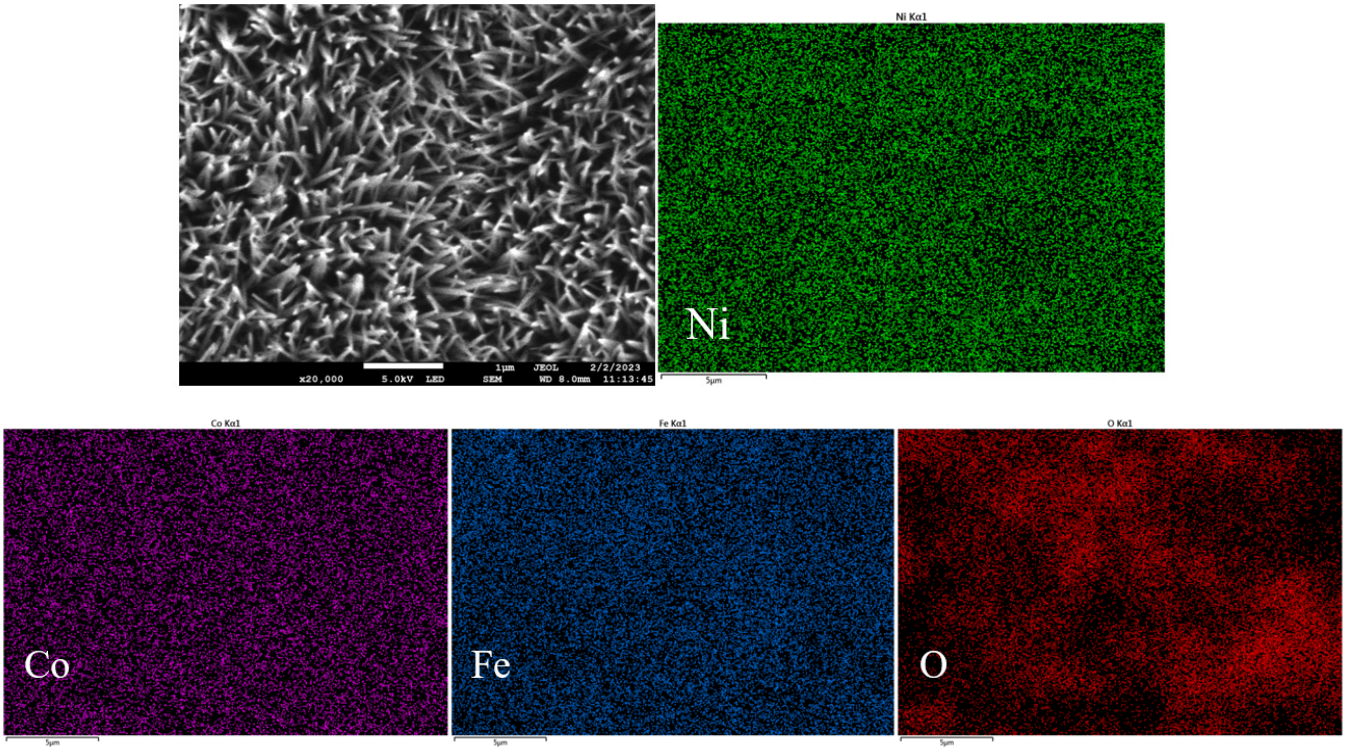

Figure 4. EDS of $Ni_4Co_4Fe_2$-LDH/NF nanoarrays.

The structure of the $Ni_4Co_4Fe_2$-LDH/NF was further confirmed by TEM analysis (Figure 5). As shown in Figure 5a, the Ni_4Co_4Fe-LDH/NF nanoneedle can be observed clearly. The high-resolution TEM (HRTEM) image (Figure 5b) shows the lattice fringes with distances of 0.132, 0.143, and 0.153 nm corresponding to the (201) plane of $Ni_{0.75}Co_{0.25}(CO_3)_{0.125}(OH)_2{\cdot}0.38H_2O$, (204) plane of $3Ni(OH)_2{\cdot}2H_2O$, and (113) plane of $Co_{5.84}Fe_{2.16}(OH)_{16}$ $(CO_3)_{1.08}{\cdot}0.32H_2O$, respectively. As shown in Figure 5c, the selected area electron diffraction (SAED) pattern shows the (113) plane for $Co_{5.84}Fe_{2.16}(OH)_{16}$ $(CO_3)_{1.08}{\cdot}0.32H_2O$, (201) plane for $Ni_{0.75}Co_{0.25}(CO_3)_{0.125}(OH)_2{\cdot}0.38H_2O$, and (316) plane for $3Ni(OH)_2{\cdot}2H_2O$, according to the JCPDF of X-ray diffraction (XRD).

The surface chemical state of $Ni_4Co_4Fe_2$-LDH/NF was investigated by XPS technique (see Figure 6). As shown in Figure 6, XPS results confirm the presence of Ni, Co, and Fe on the film surface. The binding energy peaks of Ni $2p_{3/2}$, Co $2p_{3/2}$, and Fe $2p_{3/2}$ are located at 856.4 eV, 782.2 eV, and 714.8 eV, respectively, indicating the +2, +3, and +3 oxidation states of Ni, Co, and Fe, respectively [39].

3.2. Electrochemical Characterization of the Electrocatalysts

The as-prepared Ni-Co-based LDH electrocatalysts were investigated as working electrodes for electrochemical characterization. We studied the OER performance of the electrocatalysts in a three-electrode system with 1.0 M KOH aqueous solution as the electrolyte. Electrochemical characterization of as-prepared electrocatalysts are shown in Figure 7. The polarization curves of the series of electrocatalysts after iR-drop correction are shown in Figure 7a. As can be seen in the figure, the overpotential of $Ni_4Co_4Fe_2$-LDH/NF is about 222 mV at a current density of 20 $mAcm^{-2}$, which is similar to that of NiCo-LDH/NF (361 mV), Ni_4Co_4Fe-LDH/NF (231 mV), and $Ni_4Co_4Fe_3$-LDH/NF (238 mV). Therefore, an appropriate amount of Fe doping can significantly reduce the over-

potential, which contributes greatly toward improving the electrochemical performances of the electrocatalysts.

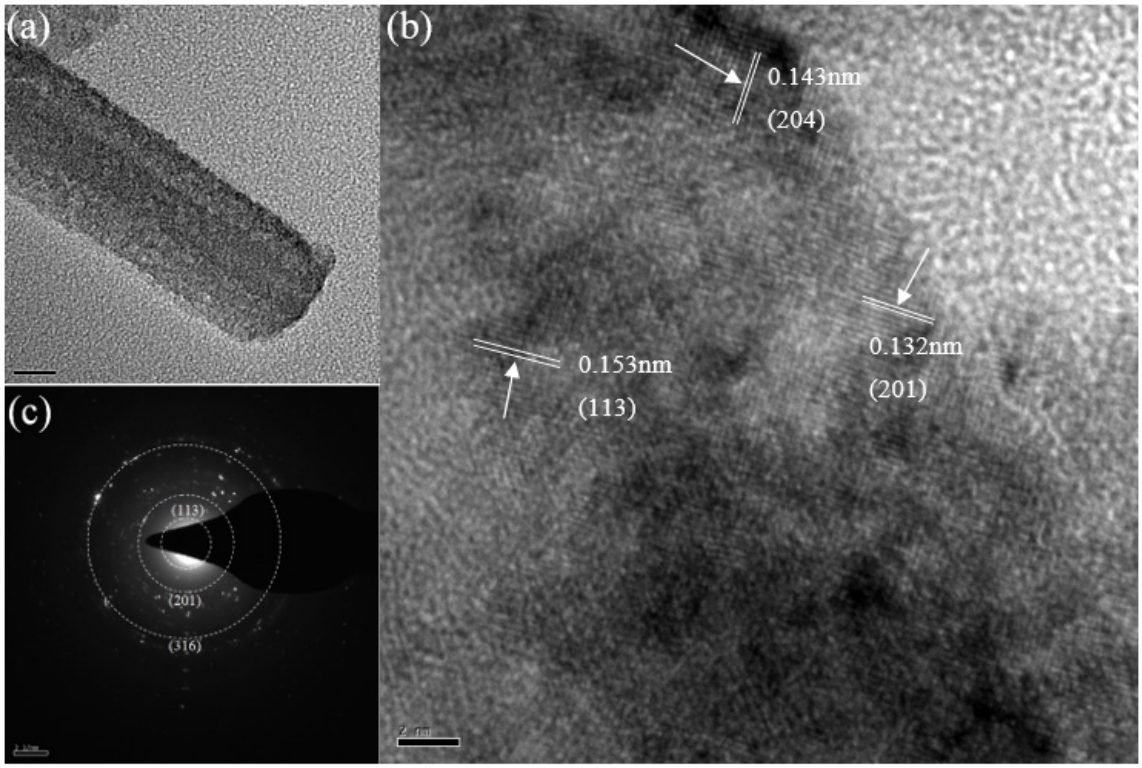

Figure 5. (**a**) TEM image, (**b**) HRTEM image, and (**c**) SAED pattern of $Ni_4Co_4Fe_2$-LDH/NF.

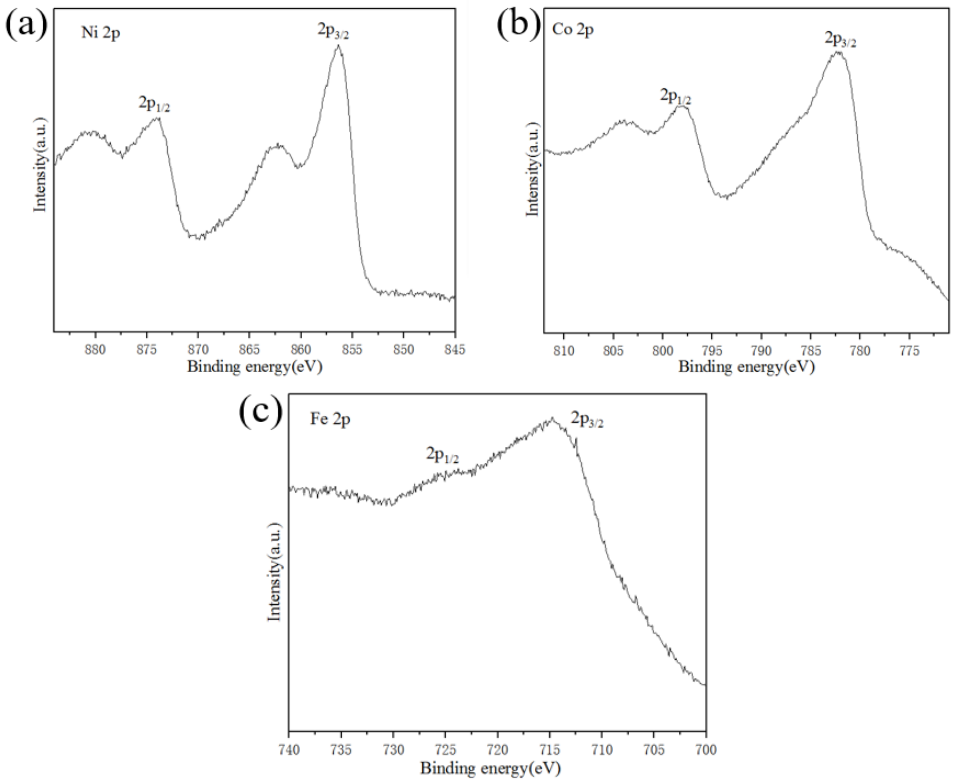

Figure 6. XPS spectra of $Ni_4Co_4Fe_2$-LDH/NF: (**a**) Ni 2p, (**b**) Co 2p, (**c**) Fe 2p.

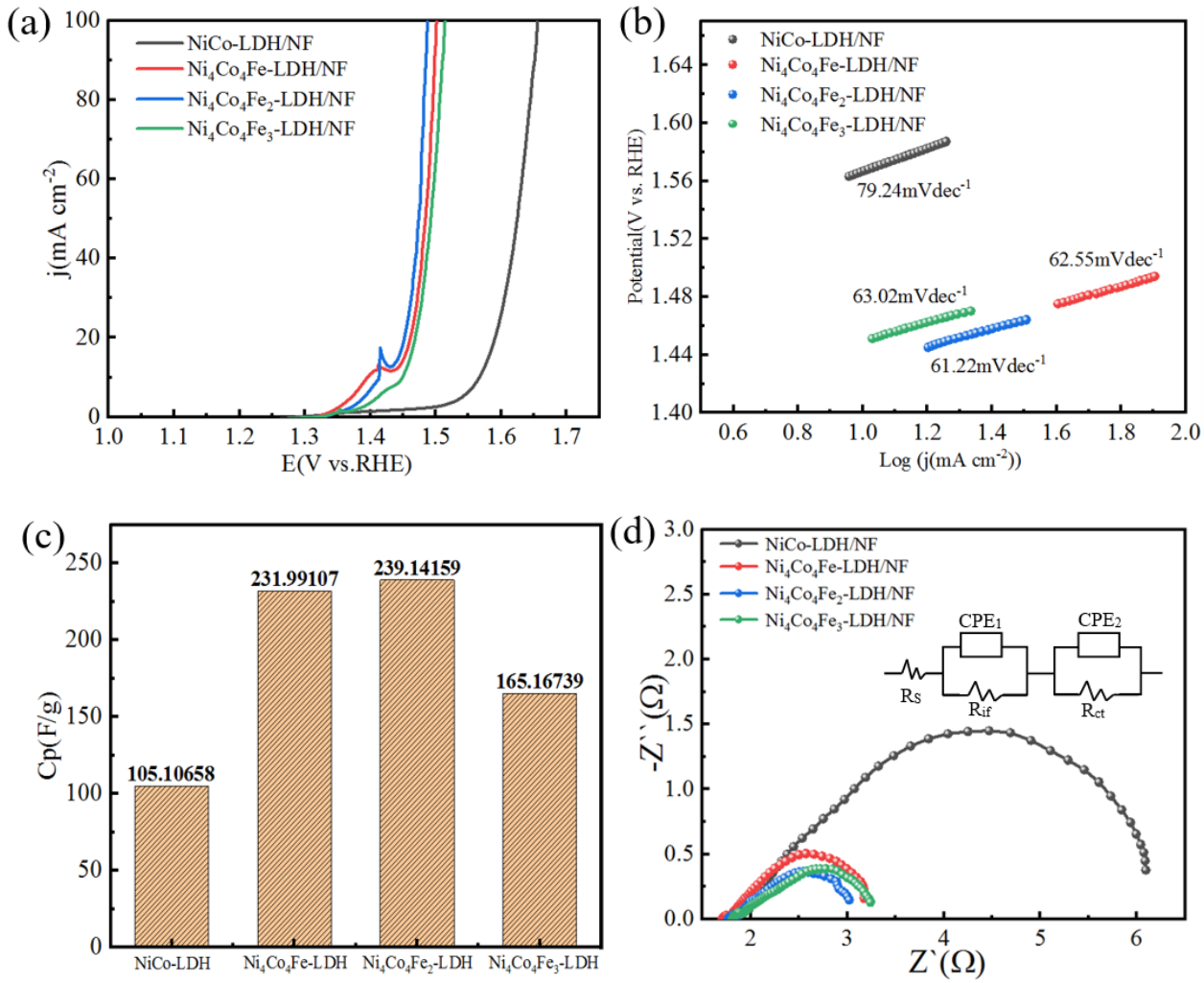

Figure 7. Polarization curves of Ni−Co based LDH electrode catalysts. (**a**) LSV curves of the electrode catalysts in an O_2−saturated 1.0 M KOH solution at the scan rate of 2 mVs^{-1}. (**b**) Tafel plot (overpotential vs. log current) derived from the corresponding polarization curves. (**c**) Specific capacitance values calculated from CV tests (as mentioned in Section 2.4). (**d**) Nyquist plots recorded at the overpotential of 1.48 V vs. RH.

In addition, the reaction kinetics of catalysts was mainly evaluated by the Tafel slope that was calculated according to the LSV curve from 1.0 to 1.7 V, as shown in Figure 7b. Obviously, $Ni_4Co_4Fe_2$-LDH/NF exhibits a Tafel slope of 61.22 $mVdec^{-1}$, which is highly competitive with NiCo-LDH/NF (79.24 $mVdec^{-1}$), Ni_4Co_4Fe-LDH/NF (62.55 $mVdec^{-1}$), and $Ni_4Co_4Fe_3$- LDH/NF (63.02 $mVdec^{-1}$). This illustrates that the facilitated reaction kinetics of OER can be realized by $Ni_4Co_4Fe_2$-LDH/NF.

The OER of electrocatalysts in alkaline solution can be accomplished through multistep reactions. Firstly, on the active sites of the catalysts, the adsorbed H_2O is transformed into some kind of [OH] intermediate. Secondly, the intermediate product [OH] is further oxidized or decomposed into [O]. Thirdly, [O] reacts with water to produce an [OOH] intermediate. Fourthly, O_2 is released from [OOH]. Please note that the square brackets above indicate an oxygen vacancy site at the surface. The OER performance of the catalysts correlate with the number of active sites and the adsorption affinity of H_2O and the intermediates [40].

The specific capacitances of the as-prepared materials are shown in Figure 7c. The specific capacitance of $Ni_4Co_4Fe_2$-LDH/NF reaches 239.1 F/g, which is significantly larger than that of NiCo-LDH/NF (105.1 F/g), Ni_4Co_4Fe-LDH/NF (232 F/g), and $Ni_4Co_4Fe_3$-

LDH/NF (165.2 F/g). Nevertheless, the Tafel slope usually reflects the apparent dynamics of the electrochemical reactions without excluding the mass transfer effect [40]. For this, EIS is adopted to assess the intrinsic dynamics of electrode. The charge transfer characteristics in the OER process at 1.48 V vs. RHE were tested.

The Nyquist plot of the as-prepared sample is shown in Figure 7d. Such a Nyquist curve should be divided into two parts, namely, the left semicircle in the high frequency range and the right semicircles in the low frequency range, suggesting the complex electrochemical process of the as-prepared samples as the OER catalysts [41]. Moreover, the equivalent circuits of the samples can be obtained based on their Nyquist curves. As shown in Figure 7d, R_s is the solution resistance, R_{ct} is the charge transfer resistance, and CPE_1 refers to the constant phase angle elements. In addition, there is a parallel connection linked by an interface resistance R_{if} element and a CPE_2. This maybe relates to the hetero-interfaces between the several composites, as shown in XRD patterns (Figure 1) [42]. Furthermore, the existence of the hetero-interfaces contributes toward reducing the charge-transfer resistance. According to the EIS results (Figure 7d), the R_{ct} of $Ni_4Co_4Fe_2$-LDH/NF (1.525 Ω) is obviously smaller than NiCo-LDH/NF (4.821 Ω), Ni_4Co_4Fe-LDH/NF (1.733 Ω), and $Ni_4Co_4Fe_3$-LDH/NF (1.765 Ω). This indicates that $Ni_4Co_4Fe_2$-LDH/NF has excellent electron transport kinetics [43–45].

The specific area and pore parameters of the samples are shown in Table 2. From Table 2, the specific area and pore volume of $Ni_4Co_4Fe_2$-LDH/NF is higher than other samples. This is favorable for improving the active site for hydrolysis reaction, and increases the efficiency of the electrocatalysts.

Table 2. Specific area and pore volume of the samples.

Sample	S_{BET} (m^2/g)	V_{total} (cm^3/g)
NiCo-LDH/NF	2.6960	0.006506
Ni_4Co_4Fe-LDH/NF	5.2154	0.014053
$Ni_4Co_4Fe_2$-LDH/NF	5.9850	0.014886
$Ni_4Co_4Fe_3$-LDH/NF	5.9727	0.012626

The C_{dl} and ECSA of Ni-Co based LDH electrode catalyst samples are shown in Figure 8. A large ECSA can provide more exposed active sites for the electrocatalytic reaction. ECSA is calculated as ECSA = C_{dl}/C_s, where C_{dl} is the electrochemical double-layer capacitance, and C_s is the specific capacitance, where C_s is usually adopted as 0.04 mF cm^{-2} for Ni-/Co-based catalysts [42]. The double-layer capacitor (Cdl) was calculated based on the cyclic voltammetry (CV). As can be seen in the figure, $Ni_4Co_4Fe_2$-LDH/NF has the highest C_{dl} and ECSA, which is attributable to the exposure of more active sites in the nanoarray, which significantly enhances the OER performance of the electrode catalyst [45].

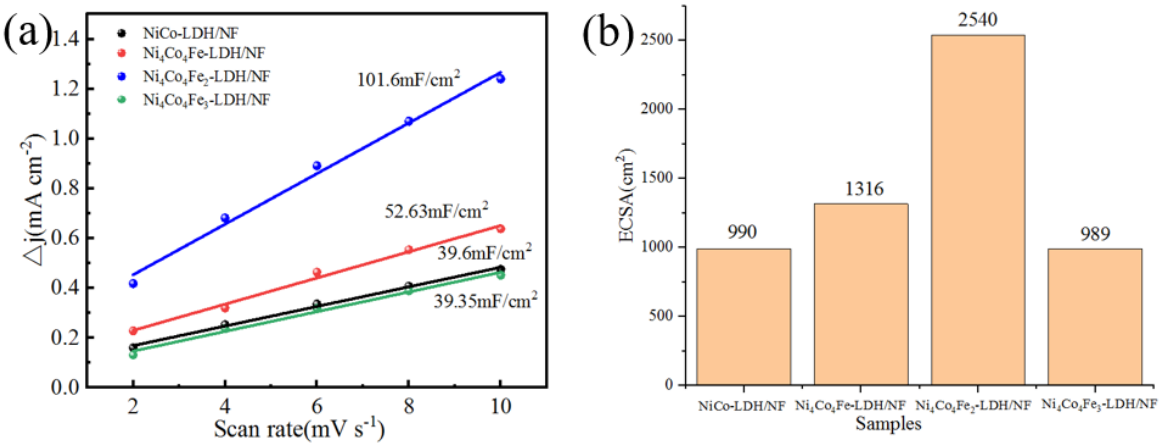

Figure 8. (**a**) C_{dl} and (**b**) ECSA of Ni−Co based LDH electrode catalysts samples.

CV curves of the as-prepared samples at a scan rate of 10 mV/s are shown in Figure 9. As can be seen in the figure, the curve of $Ni_4Co_4Fe_2$-LDH/NF shows the largest area in the series of materials, indicating that it possesses the highest specific capacitance among the four electrocatalysts. This conclusion agrees with the specific capacitance of the electrode [24].

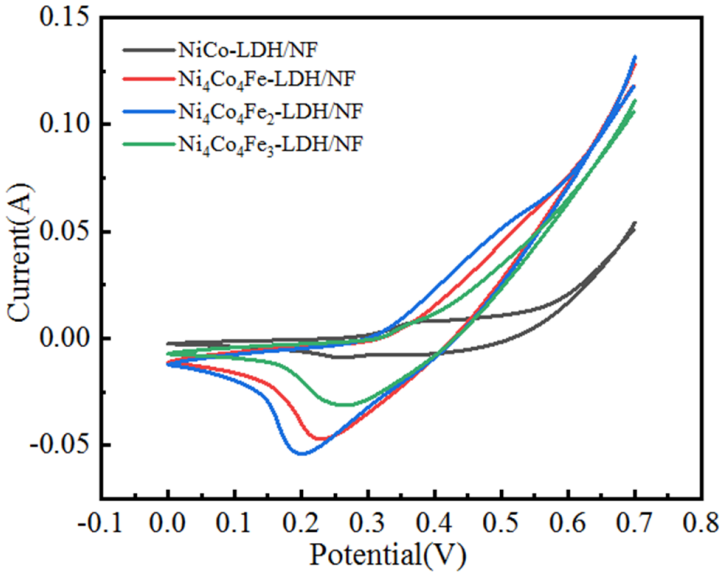

Figure 9. CV curves of Ni−Co based LDH electrode catalysts at the scan rate of 10 mV/s.

Stability is an important parameter for an electrocatalyst. Chronoamperometry was used to evaluate the electrocatalytic durability of the as-prepared electrocatalyst for OER in 1.0 M KOH. As shown in Figure 10, the V-t curve shows that after a 12 h stability test at 10 mA·cm^{-2} in alkaline solution, the potential does not significantly decrease. This suggests that $Ni_4Co_4Fe_2$-LDH/NF has excellent OER stability as an electrocatalyst. As shown in Figure 11, after a 12 h stability test, $Ni_4Co_4Fe_2$-LDH/NF still maintained its inherent morphology. The parameters of $Ni_4Co_4Fe_2$-LDH/NF after the stability test are shown in Table 3; the ratio of length/diameter is 21, which is very close to that before the stability test (Table 1). All the above factors prove its excellent stability.

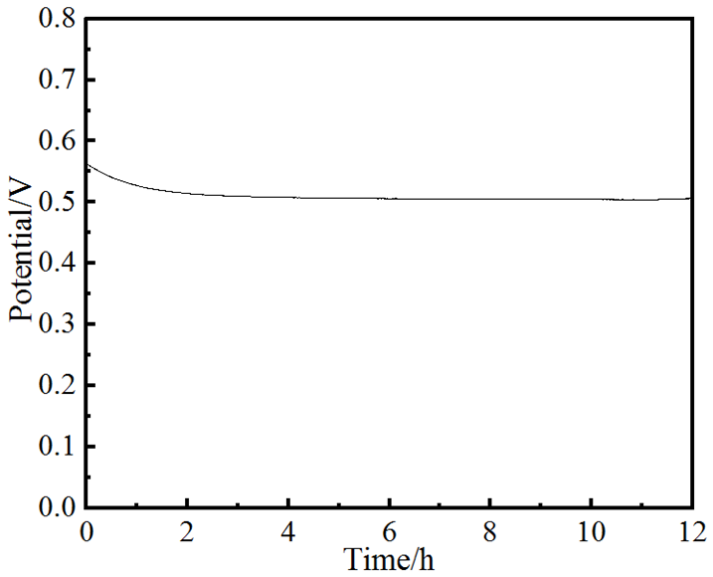

Figure 10. Chronoamperometry test of $Ni_4Co_4Fe_2$-LDH/NF at 10 mA·cm^{-2}.

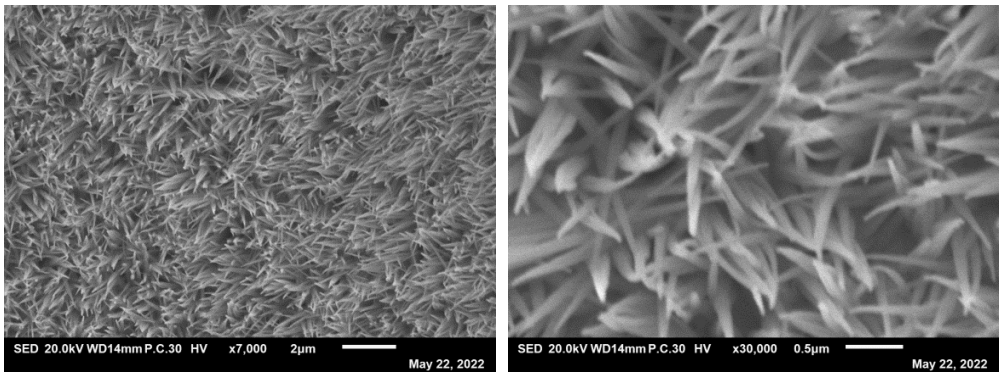

Figure 11. Morphology of $Ni_4Co_4Fe_2$−LDH/NF after the stability test.

Table 3. The parameters of $Ni_4Co_4Fe_2$-LDH/NF after the stability test.

Samples	Length (μm)	Diameter (nm)	Ratio of L/D
$Ni_4Co_4Fe_2$-LDH	0.75	35	21

A comparison of OER performance of this work with other reported NiCo-based electrocatalysts is shown in Table 4. As can be seen from the table, compared with other reported NiCo-based electrocatalysts, Fe doping can significantly change the morphology of the catalysts, which will significantly increase the active surface area of the polymetallic catalysts; it will provide more active sites for the decomposition of electrocatalytic reactions and obviously reduce the overpotential of the system [46–51].

Table 4. Comparison of OER performance of this work with other reported NiCo-based electrocatalysts.

Catalyst	Current Density ($mA\ cm^{-2}$)	Overpotential (mV)	Reference
NiCo hydroxide	10	460	[34]
NiCo-LDH	10	367	[35]
NiCo-NS	10	334	[36]
$NiCo_2O_4$ hollow microcuboids	10	277	[37]
$Ni_xCo_{2x}(OH)_{6x}$@eRG/NF	10	280	[38]
ZIF-67/CoNiAl-LDH/NF	10	303	[39]
NiCoFe-LDH arrays	10	201	This work

As mentioned above, the ternary Ni-Co-based layered double hydroxide exhibits excellent electrochemical performance compared to the binary materials.

4. Conclusions

Nickel-cobalt-based ternary layered double hydroxide nanoarrays grown on nickel foam were successfully synthesized by hydrothermal method. The as-synthesized $Ni_4Co_4Fe_2$-LDH/NF showed superior electrochemical characterization with a higher specific capacitance and excellent stability. A lower overpotential of 222 mV was obtained by using $Ni_4Co_4Fe_2$-LDH/NF as an OER catalyst at a current density of 20 $mAcm^{-2}$. The Tafel slope was 61.22 $mVdec^{-1}$, which was better than other as-prepared catalysts materials. The extraordinary electrochemical performance can be attributed to the microstructure of the materials. When doped in a moderate amount of Fe element, the length–diameter ratio of the nanorods increased from 15 to 23. $Ni_4Co_4Fe_2$-LDH/NF showed the highest C_{dl} and ECSA, so it has more active sites for the decomposition of electrocatalytic reactions and obviously reduces the overpotential of the system. This work provides a facile and effective method for fabricating Ni-Co-based ternary electrocatalysts.

Author Contributions: Conceptualization: Z.L.; methodology: Z.L. and Z.Z.; software: Z.L. and Z.Z.; validation: Z.L.; formal analysis: S.L. (Shilin Li); investigation: Z.L., Z.Z., S.L. (Shilin Li), G.H., T.H., J.C., M.J., Y.L., X.Z., S.L. (Shuaifang Li) and C.C.; data curation: G.H.; writing—original draft preparation: Z.L.; writing—review and editing: G.W.; supervision: G.W.; project administration: G.W.; funding acquisition: C.C. All authors have read and agreed to the published version of the manuscript.

Funding: This research was funded by the Student Research Train Program of Henan University of Science and Technology (No. 2022050), and the National Natural Science Foundation of China (No. 51901070).

Institutional Review Board Statement: Not applicable.

Informed Consent Statement: Not applicable.

Data Availability Statement: Not applicable.

Conflicts of Interest: The authors declare no conflict of interest.

References

1. Song, F.; Bai, L.; Moysiadou, A.; Lee, S.; Hu, C.; Liardet, L.; Hu, X. Transition metal oxides as electrocatalysts for the oxygen evolution reaction in alkaline solutions: An application-inspired renaissance. *J. Am. Chem. Soc.* **2018**, *140*, 7748–7759. [CrossRef] [PubMed]
2. Beall, C.E.; Fabbri, E.; Schmidt, T.J. Perovskite oxide based electrodes for the oxygen reduction and evolution reactions: The underlying mechanism. *ACS Catal.* **2021**, *11*, 3094–3114. [CrossRef]
3. Fabbri, E.; Nachtegaal, M.; Binninger, T.; Cheng, X.; Kim, B.-J.; Durst, J.; Bozza, F.; Graule, T.; Schäublin, R.; Wiles, L.; et al. Dynamic surface self-Reconstruction is the key of highly active perovskite nano-electrocatalysts for water Splitting. *Nat. Mater.* **2017**, *16*, 925–931. [CrossRef]
4. Cai, J.; Ding, J.; Wei, D.; Xie, X.; Li, B.; Lu, S.; Zhang, J.; Liu, Y.; Cai, Q.; Zang, S. Coupling of Ru and O-vacancy on 2D Mo-based electrocatalyst via a solid-phase interface reaction strategy for hydrogen evolution reaction. *Adv. Energy Mater.* **2021**, *11*, 2100141. [CrossRef]
5. Zhang, Z.; Wen, G.; Luo, D.; Ren, B.; Zhu, Y.; Gao, R.; Dou, H.; Sun, G.; Feng, M.; Bai, Z.; et al. Two ships in a bottle Design for Zn-Ag-O catalyst enabling selective and long-lasting CO_2 electroreduction. *J. Am. Chem. Soc.* **2021**, *143*, 6855–6864. [CrossRef] [PubMed]
6. Millán, G.G.; Hellsten, S.; Llorca, J.; Luque, R.; Sixta, H.; Balu, A.M. Recent advances in the catalytic production of platform chemicals from holocellulosic biomass. *ChemCatChem* **2019**, *11*, 2022–2042. [CrossRef]
7. Shiva Kumar, S.; Himabindu, V. Hydrogen production by PEM water electrolysis—A review. *Mater. Sci. Energy Technol.* **2019**, *2*, 442–454. [CrossRef]
8. Song, J.; Wei, C.; Huang, Z.F.; Liu, C.; Zeng, L.; Wang, X.; Xu, Z.J. A review on fundamentals for designing oxygen evolution electrocatalysts. *Chem. Soc. Rev.* **2020**, *49*, 2196–2214. [CrossRef]
9. Karmakar, A.; Karthick, K.; Sankar, S.S.; Kumaravel, S.; Madhu, R.; Kundu, S. A vast exploration of improvising synthetic strategies for enhancing the OER kinetics of LDH structures: A Review. *J. Mater. Chem. A* **2021**, *9*, 1314–1352. [CrossRef]
10. Fu, G.; Wang, Y.; Tang, Y.; Zhou, K.; Goodenough, J.B.; Lee, J.M. Superior oxygen electrocatalysis on nickel indium thiospinels for rechargeable Zn-Air batteries. *ACS Mater. Lett.* **2019**, *1*, 123–131. [CrossRef]
11. Qiu, Y.; Feng, Z.; Ji, X.; Liu, J. Surface self-reconstruction of nickel foam triggered by hydrothermal corrosion for boosted water oxidation. *Int. J. Hydrogen Energy* **2021**, *46*, 1501e8. [CrossRef]
12. Liu, Z.; Zeng, L.; Yu, J.; Yang, L.; Zhang, J.; Zhang, X.; Han, F.; Zhao, L.; Li, X.; Liu, H.; et al. Charge redistribution of Ru nanoclusters on Co_3O_4 porous nanowire via the oxygen regulation for enhanced hydrogen evolution reaction. *Nano Energy* **2021**, *85*, 105940. [CrossRef]
13. Huang, Y.; Wang, J.; Zou, Y.; Jiang, L.W.; Liu, X.L.; Jiang, W.J.; Liu, H.; Hu, J.-S. Selective Se doping of $NiFe_2O_4$ on an active NiOOH scaffold for efficient and robust water oxidation. *Chin. J. Catal.* **2021**, *42*, 1395–1403. [CrossRef]
14. Huang, Y.; Jiang, L.W.; Liu, X.L.; Tan, T.; Liu, H.; Wang, J.J. Precisely engineering the electronic structure of active sites boosts the activity of iron-nickel selenide on nickel foam for highly efficient and stable overall water splitting. *Appl. Catal. B Environ.* **2021**, *299*, 120678. [CrossRef]
15. Li, P.; Zhao, R.; Chen, H.; Wang, H.; Wei, P.; Huang, H.; Liu, Q.; Li, T.; Shi, X.; Zhang, Y.; et al. Recent advances in the development of water oxidation electrocatalysts at mild pH. *Small* **2019**, *15*, 1805103. [CrossRef] [PubMed]
16. Burke, M.S.; Enman, L.J.; Batchellor, A.S.; Zou, S.; Boettcher, S.W. Oxygen evolution reaction electrocatalysis on transition metal oxides and (Oxy)hydroxides: Activity trends and design principles. *Chem. Mater.* **2015**, *27*, 7549–7558. [CrossRef]
17. Cai, M.; Liu, Q.; Xue, Z.; Li, Y.; Fan, Y.; Huang, A.; Li, M.R.; Croft, M.; Tyson, T.A.; Ke, Z.; et al. Constructing 2D MOFs from 2D LDHs: A highly efficient and durable electrocatalyst for water oxidation. *J. Mater. Chem. A* **2020**, *8*, 190–195. [CrossRef]

18. Wang, H.; Li, J.; Li, K.; Lin, Y.; Chen, J.; Gao, L.; Nicolosi, V.; Xiao, X.; Lee, J.M. Transition metal nitrides for electrochemical energy applications. *Chem. Soc. Rev.* **2021**, *50*, 1354–1390. [CrossRef] [PubMed]
19. Tian, D.; Denny, S.R.; Li, K.; Wang, H.; Kattel, S.; Chen, J.G. Density functional theory studies of transition metal carbides and nitrides as electrocatalysts. *Chem. Soc. Rev.* **2021**, *15*, 256–264. [CrossRef]
20. Li, R.; Ren, P.; Yang, P.; Li, Y.; Zhang, H.; Liu, A.; Wen, S.; Zhang, J.; An, M. Bimetallic co-doping engineering over nickel-based oxy-hydroxide enables high-performance electrocatalytic oxygen evolution. *J. Colloid Interface Sci.* **2022**, *631*, 173–181. [CrossRef] [PubMed]
21. Liu, P.; Pu, Y. Construction of two-dimensional CoPS3@defective N-doped carbon composites for enhanced oxygen evolution reaction. *Int. J. Hydrogen Energy* **2021**, *47*, 197–202. [CrossRef]
22. Wang, X.; Wang, J.; Sun, X.; Wei, S.; Cui, L.; Yang, W.; Liu, J. Hierarchical coral-like NiMoS nanohybrids as highly efficient bifunctional electrocatalysts for overall urea electrolysis. *Nano Res.* **2018**, *11*, 988–996. [CrossRef]
23. Liu, R.; Wang, Y.; Liu, D.; Zou, Y.; Wang, S. Water-plasma-enabled exfoliation of ultrathin layered double hydroxide nanosheets with multivacancies for water oxidation. *Adv. Mater.* **2017**, *29*, 1701546. [CrossRef] [PubMed]
24. Wang, Z.; Zhang, X.; Wang, J.; Zou, L.; Liu, Z.; Hao, Z. Preparation and capacitance properties of graphene/NiAl layered double-hydroxide nanocomposite. *J. Colloid Interface Sci.* **2013**, *396*, 251–257. [CrossRef]
25. Chhetri, K.; Muthurasu, A.; Dahal, B.; Kim, T.; Mukhiya, T.; Chae, S.-H.; Ko, T.; Choi, Y.; Kim, H. Engineering the abundant heterointerfaces of integrated bimetallic sulfide-coupled 2D MOF-derived mesoporous CoS_2 nanoarray hybrids for electrocatalytic water splitting. *Mater. Today Nano* **2022**, *17*, 100146. [CrossRef]
26. Jaramillo, T.; Jørgensen, K.; Bonde, J.; Nielsen, J.; Horch, S.; Chorkendorff, I. Identification of active edge sites for electrochemical H_2 evolution from MoS_2 nanocatalysts. *Science* **2007**, *317*, 100–102. [CrossRef] [PubMed]
27. Qayum, A.; Peng, X.; Yuan, J.; Qu, Y.; Zhou, J.; Huang, Z.; Xia, H.; Liu, Z.; Tan, D.; Chu, P.; et al. Highly durable and efficient Ni-FeO_x/$FeNi_3$ electrocatalysts synthesized by a facile in situ combustion-based method for overall water splitting with large current densities. *ACS Appl. Mater. Interfaces* **2022**, *14*, 27842–27853. [CrossRef] [PubMed]
28. Solomon, E.; Baldwin, M.; Lowery, M. Electronic structures of active sites in copper proteins: Contributions to reactivity. *Chem. Rev.* **1992**, *92*, 521–542. [CrossRef]
29. Conesa, J. Electronic structure of the (undoped and Fe-doped) NiOOH O2 evolution electrocatalyst. *J. Phys. Chem. C* **2016**, *120*, 18999–19010. [CrossRef]
30. Du, X.; Huang, J.; Zhang, J.; Yan, Y.; Wu, C.; Hu, Y.; Yan, C.; Lei, T.; Chen, W.; Fan, C.; et al. Modulating electronic structures of inorganic nanomaterials for efficient electrocatalytic water splitting. *Angew. Chem. Int. Ed.* **2019**, *58*, 4484–4502. [CrossRef]
31. Ma, Y.; Chen, M.; Geng, H.; Dong, H.; Wu, P.; Li, X.; Guan, G.; Wang, T. Synergistically tuning electronic structure of porous β-Mo2C spheres by Co doping and Mo-vacancies defect engineering for optimizing hydrogen evolution reaction activity. *Adv. Funct. Mater.* **2020**, *30*, 2000561. [CrossRef]
32. Xiong, L.; Qiu, Y.; Peng, X.; Liu, Z.; Chu, P.K. Electronic structural engineering of transition metal-based electrocatalysts for the hydrogen evolution reaction. *Nano Energy* **2022**, *104*, 107882. [CrossRef]
33. Liu, H.; Guan, J.; Yang, S.; Yu, Y.; Shao, R.; Zhang, Z.; Dou, M.; Wang, F.; Xu, Q. Metal-organic-framework-derived Co2P nanoparticle/multi-doped porous carbon as a trifunctional electrocatalyst. *Adv. Mater.* **2020**, *32*, 2003649. [CrossRef]
34. Zhang, W.; Chen, G.; Zhao, J.; Liang, J.; Sun, L.; Liu, G.; Ji, B.; Yan, X.; Zhang, J. Self-growth Ni2P nanosheet arrays with cationic vacancy defects as a highly efficient bifunctional electrocatalyst for overall water splitting. *J. Colloid Interface Sci.* **2020**, *561*, 638–646. [CrossRef] [PubMed]
35. Wu, Y.; Li, F.; Chen, W.; Xiang, Q.; Ma, Y.; Zhu, H.; Tao, P.; Song, C.; Shang, W.; Deng, T.; et al. Coupling interface constructions of MoS2/Fe5Ni4S8 heterostructures for efficient electrochemical water splitting. *Adv. Mater.* **2018**, *30*, 1803151. [CrossRef]
36. Ling, C.; Shi, L.; Ouyang, Y.; Chen, Q.; Wang, J. Transition metal-promoted V2CO2(MXenes): A new and highly active catalyst for hydrogen evolution reaction. *Adv. Sci.* **2016**, *3*, 1600180. [CrossRef]
37. Chen, P.; Xu, K.; Tao, S.; Zhou, T.; Tong, Y.; Ding, H.; Zhang, L.; Chu, W.; Wu, C.; Xie, Y. Phase-transformation engineering in cobalt diselenide realizing enhanced catalytic activity for hydrogen evolution in an alkaline medium. *Adv. Mater.* **2016**, *28*, 7527–7532. [CrossRef] [PubMed]
38. Seong-Min, J.; Muthurasu, A.; Chhetri, K.; Kim, H.Y. Metal-organic framework assisted vanadium oxide nanorods as efficient electrode materials for water oxidation. *J. Colloid Interface Sci.* **2022**, *618*, 475–482.
39. Baz, A.; Holewinski, A. Predicting macro-kinetic observables in electrocatalysis using the generalized degree of rate control. *J. Catal.* **2021**, *397*, 233–244. [CrossRef]
40. Friebel, D.; Louie, M.W.; Bajdich, M.; Sanwald, K.E.; Cai, Y.; Wise, A.M.; Cheng, M.-J.; Sokaras, D.; Weng, T.-C.; Alonso-Mori, R.; et al. Identification of Highly Active Fe Sites in (Ni,Fe)OOH for Electrocatalytic Water Splitting. *J. Am. Chem. Soc.* **2015**, *137*, 1305. [CrossRef]
41. Zhang, H.; Li, X.; Hähnel, A.; Naumann, V.; Lin, C.; Azimi, S.; Schweizer, S.L.; Maijenburg, A.W.; Wehrspohn, R.B. Bifunctional heterostructure assembly of NiFe LDH nanosheets on NiCoP nanowires for highly efficient and stable overall water splitting. *Adv. Funct. Mater.* **2018**, *28*, 1706847. [CrossRef]
42. Lv, J.; Wang, L.; Li, R.; Zhang, K.; Zhao, D.; Li, Y.; Li, X.; Huang, X.; Wang, G. Constructing a hetero-interface composed of oxygen vacancy-enriched Co3O4 and crystalline–amorphous NiFe-LDH for oxygen evolution reaction. *ACS Catal.* **2021**, *11*, 14338–14351. [CrossRef]

43. Yu, M.; Budiyanto, E.; Tüysüz, H. Principles of Water Electrolysis and Recent Progress in Cobalt-, Nickel-, and Iron-Based Oxides for the Oxygen Evolution Reaction. *Angew. Chem. Int. Ed.* **2022**, *61*, e202103824.
44. Sun, H.; Xu, X.; Kim, H.; Jung, W.; Zhou, W.; Shao, Z. Electrochemical Water Splitting: Bridging the Gaps between Fundamental Research and Industrial Applications. *Energy Environ. Mater.* **2022**, e12441. [CrossRef]
45. Sun, H.; Li, L.; Chen, Y.; Kim, H.; Xu, X.; Guan, D.; Hu, Z.; Zhang, L.; Shao, Z.; Jung, W.C. Boosting ethanol oxidation by NiOOH-CuO nano-heterostructure for energy-saving hydrogen production and biomass upgrading. *Appl. Catal. B Environ.* **2023**, *325*, 122388. [CrossRef]
46. Zhao, Z.; Wu, H.; He, H.; Xu, X.; Jin, Y. A High-Performance Binary Ni-Co Hydroxide-based Water Oxidation Electrode with Three-Dimensional Coaxial Nanotube Array Structure. *Adv. Funct. Mater.* **2014**, *24*, 4698–4705. [CrossRef]
47. Liang, H.; Meng, F.; Cabán-Acevedo, M.; Li, L.; Forticaux, A.; Xiu, L.; Wang, Z.; Jin, S. Hydrothermal Continuous Flow Synthesis and Exfoliation of NiCo Layered Double Hydroxide Nanosheets for Enhanced Oxygen Evolution Catalysis. *Nano Lett.* **2015**, *15*, 1421–1427. [CrossRef] [PubMed]
48. Song, F.; Hu, X. Exfoliation of layered double hydroxides for enhanced oxygen evolution catalysis. *Nat. Commun.* **2014**, *5*, 4477. [CrossRef]
49. Gao, X.; Zhang, H.; Li, Q.; Yu, X.; Hong, Z.; Zhang, X.; Liang, C.; Lin, Z. Hierarchical $NiCo_2O_4$ Hollow Microcuboids as Bifunctional Electrocatalysts for Overall Water-Splitting. *Angew. Chem. Int. Ed. Engl.* **2016**, *55*, 6290–6294. [CrossRef]
50. Shi, J.; Du, N.; Zheng, W.; Li, X.; Dai, Y.; He, G. Ultrathin Ni-Co double hydroxide nanosheets with conformal graphene coating for highly active oxygen evolution reaction and lithium ion battery anode materials. *Chem. Eng. J.* **2017**, *327*, 9–17. [CrossRef]
51. Xu, J.; Zhao, Y.; Li, M.; Fan, G.; Yang, L.; Li, F. A strong coupled 2D metal-organic framework and ternary layered double hydroxide hierarchical nanocomposite as an excellent electrocatalyst for the oxygen evolution reaction. *Electrochim. Acta* **2019**, *307*, 275–284. [CrossRef]